Astronomy & Astrophysics manuscript no.
(will be inserted by hand later)

Non-LTE line formation for Mg I/II: abundances and stellar parameters

Model atom and first results on A-type stars *

N. Przybilla[1,2], K. Butler[1], S.R. Becker[1], and R.P. Kudritzki[1,2,**]

[1] Universitäts-Sternwarte München, Scheinerstraße 1, D-81679 München, Germany
[2] Max-Planck-Institut für Astrophysik, Karl-Schwarzschild-Straße 1, D-85740 Garching bei München, Germany

Received / Accepted

Abstract. An extensive model atom for non-LTE line-formation calculations for neutral and singly-ionized magnesium is presented, taking into account recent improvements in the atomic data. As a test and first application of the model, stellar parameters and magnesium abundances are determined on the basis of line-blanketed LTE model atmospheres for three stars: Vega (A0 V), η Leo (A0 Ib) and HD 92207 (A0 Iae) using high S/N and high resolution spectra at visual and near-IR wavelengths. The ionization equilibrium of Mg I/II proves to be a sensible temperature indicator for early A-type stars at all luminosities. Evidence is given that in late A and early F-type supergiants ($T_{\rm eff} \lesssim 8000$ K) the determination of accurate stellar parameters is hampered by the presence of a pressure inversion region in the model atmospheres at line-formation depths. The Mg I/II lines in the observations are reproduced simultaneously by the calculated line profiles with high accuracy. For Vega spectral synthesis in the UV region of the Mg I/II resonance lines also proves excellent consistency with the results from the visual. The dependence of the non-LTE effects on the atmospheric parameters is discussed with special emphasis on the supergiants where a strong radiation field at low particle densities favours deviations from LTE, especially in the minor ionic species of neutral magnesium. Non-LTE corrections turn out to be small in Mg I – typically $\lesssim 0.3$ dex – even in supergiants, but are essential for an accurate effective temperature determination. From the Mg II spectrum, only the features at $\lambda\lambda$ 4481 and 7877-96 Å react sensitively to non-LTE effects. Furthermore, the influence of microturbulence on the statistical-equilibrium calculations is investigated. The line strengths are found to be systematically affected.

Key words. Atomic data – Line: formation – Stars: abundances, fundamental parameters, supergiants

1. Introduction

Magnesium is *the* species of choice for the determination of stellar α-element abundances. Several strong lines of neutral or singly ionized magnesium (or of both) are present in the UV/visual spectra at all spectral types. In particular, the unblended Mg II λ 4481 line is a prominent feature in luminous BA-type supergiants. It is easily detected, even in objects well outside the Local Group which become accessible to low-resolution spectroscopy in the era of ground-based 8m-class telescopes (see Bresolin et al. 2001). Non-LTE effects play an important rôle in the line formation and have to be accounted for in a quantitative analysis (Mihalas 1972, Snijders & Lamers 1975, Sigut & Lester 1996), especially in the strong radiation field of supergiants.

In combination with abundances of the iron peak elements, this offers the opportunity to study the cosmochemical evolution of a large number of galaxies. The primary source for the enrichment of α-elements in the interstellar medium are supernova type II events, while iron peak elements are released in supernovae of high and low mass stars. Thus, knowledge of abundance ratios also helps to constrain the star-formation history. Direct observational evidence for this is given by the α-enhancement found in galactic Population II stars (e.g. Fuhrmann 1998).

The simultaneous presence of magnesium lines of the neutral and singly-ionized species in A and F-type stars also offers the opportunity to determine their effective temperatures from the ionization equilibrium as an alternative to purely photometric or spectrophotometric methods. In combination with the fitting of the line wings of the higher members of the Balmer series, the slight dependence of the ionization equilibrium on surface gravity can be overcome. This purely spectroscopic approach was recently used by Venn (1995, 1999) and Venn et al. (2000, 2001) to derive the stellar parameters for

Send offprint requests to: N. Przybilla (nob@usm.uni-muenchen.de)

* Based on observations collected at the European Southern Observatory, La Silla, Chile (ESO N° 62.H-0176)

** *Present address:* Institute for Astronomy, University of Hawaii, 2680 Woodlawn Drive, Honolulu, HI 96822

galactic and extragalactic (SMC, M31, NGC 6822) supergiants. Here, non-LTE effects influence the ionization balance by overionization of the minor ionic species, Mg I, again an effect most pronounced in supergiants. The studies are based on the non-LTE model atom from Gigas (1988), extensively tested on the main sequence star Vega. Meanwhile, improved line-blanketed model atmospheres have become available (Kurucz 1991) and the accuracy of atomic data has been enhanced enormously due to the efforts of e.g. the Opacity Project (OP; see Seaton et al. (1994) for a general overview). The wealth of available atomic data has been facilitated by the simplicity of the atomic structure, which allows good theoretical modeling. A critical reinvestigation therefore seems appropriate in order to determine the possibilities for improving the accuracy of abundance and stellar parameter determinations.

Several other interesting topics can be investigated by using strong magnesium lines. In the early-type stars, the UV lines are tracers for stellar outflow, with velocity fields altering the line profiles dramatically (e.g. Talavera & Gomez de Castro 1987, Verdugo et al. 1999). Terminal wind velocities for A-type supergiants are preferentially derived from the violet extent of the black absorption troughs of the Mg II resonance lines (Lamers et al. 1995). At later spectral types than studied here, the Mg b lines become a sensitive diagnostic tool for surface gravity determination (e.g. Deeming 1960). Sophisticated model atoms for Mg I find only quite small deviations from LTE in the sun, but these are essential for the interpretation of the infrared Mg I emission features (Carlsson et al. 1992, Zhao et al. 1998). By analogy, Sigut & Lester (1996) predict similar features for Mg II Rydberg transitions in B-type stars.

This paper concentrates on the accurate abundance and stellar temperature determination from observed Mg I/II lines in A-type stars with special emphasis on supergiants. A comprehensive model atom for Mg I/II is presented in the next section, together with a critical examination of the expected uncertainties. The results from our LTE and non-LTE line-formation computations are discussed in Sect. 3. In the following section, the atmospheric parameters and magnesium abundances for a test sample of three stars are determined from high S/N and high resolution spectra. Finally, a short summary is given in Sect. 5.

The application of the model to the determination of stellar parameters and magnesium abundances in extragalactic supergiants (see Herrero et al. (2000) for first results) will be the subject of further investigation. An implementation of the model atom for the hydrodynamic radiative transfer code of Santolaya-Rey et al. (1997) is also intended for a quantitative analysis of the stellar wind dominated Mg II resonance lines of supergiants.

2. Model calculations

2.1. Model atmospheres and programs

The calculations are performed using the standard assumptions of plane-parallel, homogeneous and stationary stellar atmospheres in hydrostatic and radiative equilibrium. Magnesium is a trace element; in the A star regime its contribution to the overall opacity is negligible. Thus we obtain statistical-equilibrium populations for Mg I/II while keeping the atmospheric parameters fixed.

The non-LTE Mg I/II line profiles are computed on the basis of ATLAS9 (Kurucz 1979, 1991) LTE line-blanketed model atmospheres using LTE Opacity Distribution Functions (ODFs, Kurucz 1992) to account for line blocking in the spectrum synthesis. For the calculation of model atmospheres for the most extreme supergiants close to the Eddington limit, modifications in the treatment of opacities and the radiative pressure in the outermost depth points within ATLAS9 were made in order to achieve convergence. Comparisons at stellar parameters for which standard ATLAS9 converges have shown that the stratification deeper in the atmosphere is only marginally affected by these modifications.

With the assumptions cited above, reliable analyses can be performed in the given temperature range from main sequence stars through to bright giants, as indicated by Kudritzki (1988). At spectral types later than ∼A7 V, an outer convection zone becomes increasingly important for the energy transport through the atmosphere, as the observation of chromospheres in these stars indicates; see e.g. Simon & Landsman (1997) for recent results. Convection is therefore taken into account in the standard way for ATLAS9 atmospheric models with $T_{\rm eff} < 8500$ K, applying a value $\ell/h = 1.5$ (mixing length to scale height).

At slightly lower temperatures ($T_{\rm eff} \lesssim 8000$ K), hydrostatic model atmospheres for supergiants develop a pressure inversion layer which eventually extends into the line-formation region. Here our line-formation calculations are expected to be hampered by systematic effects on the stellar parameter determination, see Sect. 3.3 for details.

A thorough discussion of the possible deviations from the standard assumptions on the model atmosphere structure of supergiants is given by Venn (1995). Additionally, non-LTE effects are often less significant for the model structure than is line blanketing, as demonstrated by Przybilla (1997). However, close to the Eddington limit (luminosity classes Iae and Ia$^+$) further studies on this topic are desireable; however, appropriate theoretical models are still unavailable.

The line-formation calculations are performed using the programs DETAIL and SURFACE (Giddings 1981, Butler & Giddings 1985), with the former solving the radiative transfer and the statistical-equilibrium equations and the latter computing the emergent flux. Recent improvements by inclusion of an ALI scheme (using the treatment of Rybicki & Hummer 1991) allow the utilisation of quite elaborate model atoms while the necessary computational resources remain low (typically ∼30 min CPU time for model convergence on a PC).

2.2. The model atom

2.2.1. Energy levels

The atomic model for magnesium has to be fairly complete in order to use the ionization balance of Mg I/II as a temperature indicator *and* for the determination of accurate elemental abundances. The main ionization stage at line-formation depths in the A-type stars is Mg II, with the exception of the early A-type

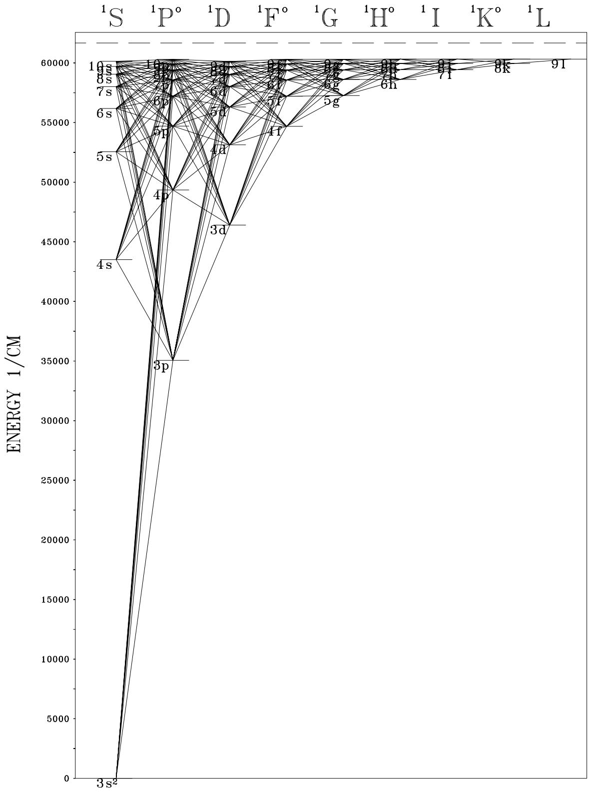

Fig. 1. Grotrian diagram for the Mg I singlet system. Displayed are the radiative transitions treated explicitly in the non-LTE calculations.

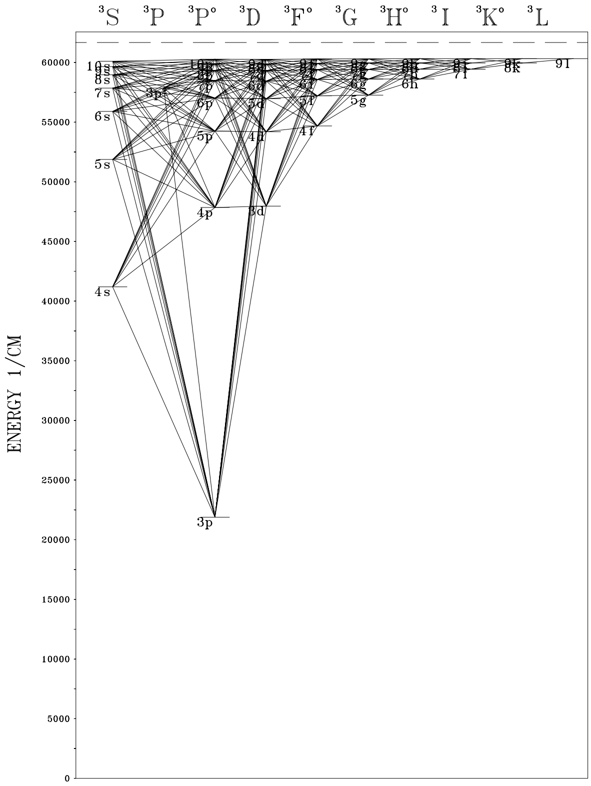

Fig. 2. Grotrian diagram for the Mg I triplet system.

supergiants where the Mg III population becomes comparable. Non-LTE effects are expected to be of importance for the interpretation of the Mg I lines and for Mg II lines emerging from highly excited levels.

Energy levels up to $\sim$0.2/0.5 eV below the ionization threshold are therefore explicitly included in our Mg I/II model as listed by Martin & Zalubas (1980). Missing states at high orbital angular momentum number ℓ are calculated using a polarization theory (Chang & Noyes 1983). This includes all energy levels with principal quantum number $n \leq 9$ and the $10s$ and $10p$ states in Mg I and all levels with $n \leq 10$ and $\ell \leq 4$ in Mg II. Only the ground state of Mg III is considered, as excited levels of Mg III are seperated by a large energy gap of $\sim$53 eV. Fine structure splitting is not taken into account: sub-levels belonging to the same term are combined into a single level.

Additionally, the remaining level populations of Mg I and Mg II up to $n = 12$ and $n = 10$, respectively, are computed in LTE relative to the ground state of the higher ionization stage with energies derived from their quantum defects. They are considered only in the number conservation equation.

2.2.2. Radiative transitions

All optically allowed bound-bound transitions between energy levels with non-LTE populations are considered. The required LS-coupling oscillator strengths are adopted from OP data (Butler et al., 1990, 1991, 1993) for Mg I and K.T. Taylor (available only from the TOPBASE database (Cunto & Mendoza 1992)) for Mg II. Missing data are calculated in the Coulomb approximation (Bates & Damgaard 1949). In order to improve the computational efficiency, the individual lines of a multiplet are reduced to a single effective "multiplet line".

Grotrian diagrams for the singlet and triplet spin systems of Mg I and for Mg II are displayed in Figs. 1-3. The non-LTE calculations are performed simultaneously for Mg I/II. Additional radiative coupling between both spin systems of Mg I is provided by the intercombination transitions $3s^2\ ^1S$ – $3p\ ^3P$, $3p\ ^3P$ – $3d\ ^1D$, – $4d\ ^1D$, – $5d\ ^1D$, – $6d\ ^1D$ and $3p\ ^1P$ – $3d\ ^3D$ with a mean gf-value from Wiese et al. (1969) and Moccia & Spizzo (1988) for the first transition and from Kurucz & Peytremann (1975) for the latter transitions. A detailed comparison of the adopted oscillator strengths with theoretical work by other authors is performed by Butler et al. (1993); the majority of the data is expected to be accurate to within 10%, superseding most of the older data used in previous studies of non-LTE effects on Mg I. A similar accuracy in the radiative data has to be expected for the Mg II ion.

Photoionizations from all energy levels with non-LTE populations are treated using detailed cross-sections from the Opacity Project (Butler et al. 1993) for Mg I and K.T. Taylor (available only from the TOPBASE database (Cunto & Mendoza 1992)) for Mg II. A carefully chosen frequency grid

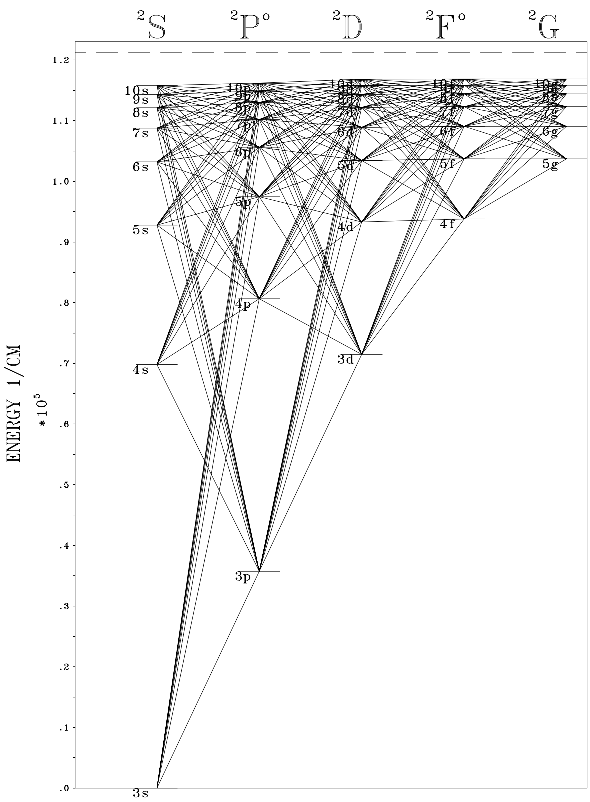

Fig. 3. Grotrian diagram for Mg II.

ensures a thorough representation of the numerous resonances present in the results of the R-matrix calculations for Mg I. Butler et al. (1993) discuss the reliability of the cross-sections for the first three states of Mg I in the context of the available experimental data and theoretical results from the literature; fairly good agreement is found. A new theoretical study of the photoionization from the ground state of Mg I (Kim & Tayal 2000) confirms the reliability of the OP data. Butler et al. (1993) expect the accuracy of the rest of the Mg I photoionization cross-sections to be high. For test purposes we assume an accuracy of $\pm 10\%$. This accuracy we also expect for the photoionization data for Mg II. Cross sections for energy levels missing in the OP data (at high ℓ) are calculated in the hydrogenic approximation (Mihalas 1978, p. 99). In summary, the use of the detailed OP data significantly improves the description of the photoionization processes compared to previous Mg I/II non-LTE studies.

In the first step of the computations, i.e. in DETAIL, the level populations are calculated using depth-dependent Doppler profiles assuming LS coupling; microturbulence is explicitly included as an additional term in the Doppler width ($\Delta\lambda_{\rm D}$):

$$\Delta\lambda_{\rm D} = \frac{\lambda_0}{c}\sqrt{v_{\rm th}^2 + \xi^2} \qquad (1)$$

where λ_0 is the rest wavelength of the transition, c the speed of light, $v_{\rm th}$ the thermal velocity for the chemical species of interest and ξ the microturbulent velocity; see Sect. 3.2 for a discussion. Both continuous opacities and ATLAS9 line-distribution functions are accounted for in solving the radiation transfer.

These LS-coupling populations are then split according to the statistical weights of the individual sub-levels in order to calculate line profiles via the program SURFACE. In this step of the calculation, Voigt profile functions are adopted and the same microturbulent velocity as in DETAIL is applied. Wavelengths are taken from Kaufman & Martin (1991) and transition probabilities from several sources, as indicated in Table 3. The damping parameters are calculated from OP radiative lifetimes (Butler et al. 1991) for the radiative widths and adopted from Dimitrijević & Sahal-Bréchot (1996) and Griem (1964,1974) for electron impact and ion broadening in Mg I/II. Missing collisional damping data are computed from the approximation of Cowley (1971). Van der Waals damping can be neglected in the parameter range considered here, as tests at the lower $T_{\rm eff}$ boundary of $\sim$8000 K have shown.

2.2.3. Collisional transitions

Only a few detailed data on collisional excitation are available for magnesium from the literature. We adopt collisional cross-sections from Clark et al. (1991) for Mg I and effective collision strengths from Sigut & Pradhan (1995) for Mg II transitions. The authors compare the data with those of previous experimental and theoretical studies and find, in general, good agreement. The expected errors are in the range of 20-30% with some being as small as 10%. For the remaining bulk of the transitions, approximate formulae must be used, giving threshold values accurate to a factor of 2-3 at best. Van Regemorter's formula (Van Regemorter 1962) is applied for radiatively permitted transitions with OP oscillator strengths. In Mg II the effective gaunt factor is set to 0.2 for all transitions, following Sigut & Lester (1996). For the optically forbidden transitions, the semiempirical Allen formula (Allen 1973) is used with the collision strength set to 1.0.

Experimental cross sections from Freund et al. (1990) and Crandall et al. (1982) are adopted for the collisional ionization of the ground states of Mg I and Mg II, respectively. These authors expect an accuracy of $\pm 10\%$ for the measurements. All the remaining collisional ionization data are computed using the Seaton formula (Seaton 1962) with threshold photoionization cross sections from the OP data where available or from the hydrogenic approximation.

2.3. Background opacities

The stellar radiation field is strongly affected by continuous and line opacities which must be correctly accounted for in the statistical-equilibrium calculations. We explicitly include bound-free opacities for the following atoms: H, He, C, N and O with abundances determined from lines in the visual and near-IR. Level populations for the first two elements are calculated in non-LTE using updated versions of the model atoms of Husfeld et al. (1989). Besides hydrogen (Lyman edge), C I is the most important continuous opacity source in the far-UV.

Its sensitivity to non-LTE has a notable impact on the stellar flux at these wavelengths (see Lemke & Venn 1996). Non-LTE populations for C I are therefore determined from a comprehensive model atom (Przybilla et al. 2001a). Where necessary an additional iteration step in the determination of the stellar parameters is introduced. Neutral oxygen and nitrogen populations are determined using the model atoms of Przybilla et al. (2000, 2001b).

Line opacities are represented by LTE ODFs (Kurucz 1992) for the appropriate metallicity and microturbulence. The original sawtooth pattern is transformed into a step function by averaging over the 10 Å-wide intervals. This procedure meets the requirements for calculating the radiation field as a whole. However, at certain important wavelengths a more detailed description is desirable. In particular, the line opacity between the Balmer jump and ∼3800 Å is poorly reproduced as the higher Balmer lines gradually merge into the continuum. The photoionizations from the Mg I $3p\ ^1P$ state (at a threshold wavelength of 3756.6 Å) might be affected by this, explaining some of the problems with fitting the spectral lines originating from this level. Except for this, no other photoionization edges or important lines of Mg I/II are situated at wavelengths with uncertain background opacities.

Despite our success in reproducing the observations, our calculations might be affected by a systematic effect neglected in the atmosphere modeling. Non-LTE effects will cause an overionization of the relevant elements in the opacity determination. The backwarming introduced by line blanketing might therefore be overestimated in LTE, as well as the magnitude of line blocking. First calculations of non-LTE line-blanketed model atmospheres for main sequence A-types (Hubeny & Lanz 1993) indicate some changes in the expected direction but adequate models for the more interesting case of supergiants are still lacking. Also, the line-blocking effects will change in non-LTE.

2.4. Error estimates for the magnesium non-LTE calculations

To assess the importance of various parameters entering the non-LTE computations and to estimate systematic errors on the effective temperature determination and abundance analysis, test calculations were performed for typical atmospheric parameters of early A-type stars: a main sequence model with 9500 K/4.0 at ξ=2 km s^{-1} and a supergiant model with 9500 K/1.5 at ξ=4 km s^{-1} assuming solar metallicity. Below $T_{\rm eff}$≈8000 K the hydrostatical model atmospheres for supergiants develop pressure inversion and should therefore – as well as for other reasons – be viewed with caution as a reliable description of the physical conditions, see Sect. 3.3. For a given synthetic spectrum of magnesium, the abundance is adjusted in the model with modified parameters to reproduce the original line strengths. The results of the tests (mean values from several lines used in abundance analyses) are summarised in Table 1.

Two important conclusions can be drawn from this. First, for the given model atom, uncertainties in the atomic data are

Table 1. Uncertainties in the non-LTE analysis of magnesium

		changes in $\log\varepsilon(\mathrm{Mg})_{\rm NLTE}$			
		9500/4.0		9500/1.5	
		Mg I	Mg II	Mg I	Mg II
Atmospheric parameters:					
$T_{\rm eff}$ − 150 K	$\sigma_{T_{\rm eff}}$	−0.11	−0.01	−0.18	−0.03
$\log g$ + 0.15 dex	$\sigma_{\log g}$	−0.06	−0.01	−0.16	−0.05
ξ +1 km s^{-1}	σ_ξ	−0.10	−0.03	−0.02	−0.07
[M/H] − 0.2 dex	$\sigma_{\rm [M/H]}$	−0.01	±0.00	−0.01	+0.02
Line transitions:					
Oscillator strengths +10%	$\sigma_{\log gf}$	−0.04	−0.04	−0.02	±0.00
Damping constant ∗2	$\sigma_{\rm damp}$	−0.05	−0.05	±0.00	±0.00
Photoionizations:					
Cross-sections +10%	$\sigma_{\rm rbf}$	±0.00	±0.00	±0.00	±0.00
Cross-sections ∗5		+0.03	+0.03	−0.01	±0.00
Collisional transitions:					
Cross-sections ∗0.1		+0.02	−0.02	+0.01	+0.01
Cross-sections ∗0.5	$\sigma_{\rm cbb}$	+0.01	−0.01	+0.01	+0.01
Cross-sections ∗2	$\sigma_{\rm cbb}$	±0.00	+0.01	−0.02	−0.01
Cross-sections ∗10		+0.01	+0.03	−0.01	−0.01
Collisional ionization:					
Cross-sections ∗0.1	$\sigma_{\rm cbf}$	±0.00	±0.00	+0.01	+0.01
Cross-sections ∗10	$\sigma_{\rm cbf}$	±0.00	±0.00	−0.04	−0.02
Continuum placement	$\sigma_{\rm cont}$	±0.05	±0.05	±0.05	±0.05
Estimated total uncertainty	$\sigma_{\rm sys}$	±0.18	±0.09	±0.25	±0.11

not a critical issue. Uncertainties in the oscillator strengths have the greatest impact and our model certainly benefits from the highly accurate OP data. In the main sequence model, the line-broadening parameters also become important due to the higher particle densities in its atmosphere. Quite accurate data are available in this case. This relative insensitivity of our magnesium model to the atomic parameters corresponds to the small non-LTE corrections found from the comparison with observations.

The second conclusion is the strong dependence of the ionization equilibrium of Mg I/II on the atmospheric parameters. As the major ionization stage of Mg II turns out to be quite insensitive to variations in $T_{\rm eff}$ and $\log g$ – and therefore should be viewed as the preferable abundance indicator – the Mg I populations react differently. Even small changes are reflected. Hence, this delicate ionization balance is an ideal tool for stellar parameter determination. The temperature sensitivity is highest but for supergiants the dependence on surface gravity becomes comparable. In either case, one can profit from this sensitivity only so long as the atmospheric models reliably reflect the local conditions in the star. For models close to the Eddington limit, this will need further investigation.

Lines of intermediate strength are most affected by microturbulence. Weak lines with equivalent widths $\lesssim$ 100 mÅ should be preferred for the analyses. For further discussion concerning this parameter, see Sect. 3.2.

Metallicity has only small effects on the magnesium populations. We achieved the appropriate changes in the background opacities by choosing ODFs for elemental abundances reduced by typical uncertainties. On the other hand, line blocking is an

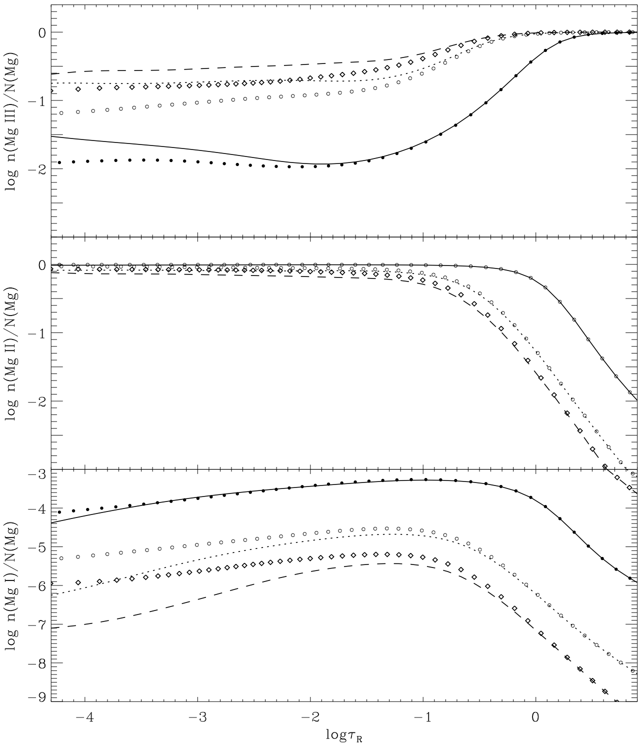

Fig. 4. Non-LTE and LTE ionization balance of magnesium for the sample stars of Sect. 4: Vega (solid lines/filled circles), η Leo (dotted lines/open circles) and HD 92207 (dashed lines/open diamonds). Displayed are the ratios of the total level populations of the three ionization stages n(Mg I/II/III) to the total magnesium population N(Mg) as a function of Rosseland optical depth $\tau_{\rm R}$. Note the non-LTE overionization of Mg I in the supergiant models and the overpopulation of Mg III.

important ingredient for the statistical-equilibrium calculations and must not be neglected.

Another source of systematic error is the continuum placement in the observed spectra. This strongly depends on the S/N ratio obtained. Our estimate in Table 1 should be applicable to high quality data with S/N $\gtrsim$ 100 only. In general, equivalent widths studies are more susceptible to this systematic error than the spectrum synthesis technique, which also accounts for the continuum regions explicitly.

The total uncertainties are computed from the sum of the squares of the appropriate uncertainties listed above, assuming them to be independent:

$$\sigma^2_{\rm sys} = \sigma^2_{T_{\rm eff}} + \sigma^2_{\log g} + \sigma^2_{\xi} + \sigma^2_{\rm [M/H]} + \sigma^2_{\log gf} + \sigma^2_{\rm damp} + \sigma^2_{\rm rbf} + \sigma^2_{\rm cbb} + \sigma^2_{\rm cbf} + \sigma^2_{\rm cont} \quad (2)$$

They should be viewed as the systematic errors applicable to our non-LTE calculations on Mg I/II *within* our methodology (cf. Sect. 2.1).

3. Discussion

In this section we evaluate the advantages of time-consuming non-LTE calculations over a straightforward LTE analysis for the interpretation of the Mg I/II spectra of A-type stars. The nature of the non-LTE effects is discussed for the stars of our test sample in Sect. 4. The influence of the microturbulence parameter on the line-formation calculations is then studied. Some comments on the impact of pressure inversion in model atmospheres below $T_{\rm eff} \sim 8000$ K on the determination of the stellar parameters are given next. Finally, our results are compared with those of a previous study of non-LTE effects in magnesium.

3.1. The non-LTE effects

The ionization balance of magnesium in the photospheres of typical early A-type stars is displayed in Fig. 4. Only a small fraction (a few parts in ten thousand) of magnesium remains neutral in the main sequence object and this is reduced by a further 1 to 2 orders of magnitude in supergiants. In the Vega model, Mg II is the dominant ionization stage throughout the line- and continuum-formation region; deeper in the atmosphere Mg III prevails. This pattern is shifted to lower optical depths in supergiants and the Mg II$\rightarrow$Mg III transition already occurs in the line-formation region. The non-LTE computations indicate an overionization of the material in the supergiant models, most notably in Mg I. For Vega, only small deviations from LTE are found in the ionization balance.

Departure coefficients $b_i = n_i^{\rm NLTE}/n_i^{\rm LTE}$ (the n_i denoting the level populations) for energy levels i are displayed in Fig. 5 as a function of the Rosseland optical depth $\tau_{\rm R}$ for our models of the objects discussed in Sect. 4. The lower levels involved in the transitions giving rise to all the observed Mg I lines in the visual/near-IR have rather low excitation energies of 2.71 eV (3p ^{3}P$^{\rm o}$) and 4.35 eV (3p ^{1}P$^{\rm o}$). The corresponding Mg II lines originate from the 3d and the $n = 4$ levels ($\gtrsim$ 8.8 eV above the ground state). Additional features in the UV also give information about the ground states of both ionization stages. In particular, the whole sequence 3s–3p–3d–4f of Mg II is sampled, giving rise to prominent absorption features.

Deep in the atmosphere, the departure coefficients approach unity as the density increases and collisional processes dominate, enforcing LTE (inner boundary condition). Farther out, marked deviations from LTE occur, setting in at larger $\tau_{\rm R}$ and being more pronounced in supergiants. Non-LTE corrections are expected to be small for Mg I as the departure coefficients deviate only slightly from unity at line-formation depths. In addition, the line formation is progressively shifted to deeper layers with decreasing surface gravity at comparable effective temperatures, thus compensating for the stronger deviations of the b_i. The energetically low-lying Mg I levels are systematically depopulated by photoionizations, resulting in $b_i < 1$. We test this by replacing the mean intensity with the Planck function, $J_\nu = B_\nu$, for the photoionization continua in our η Leo model, thus eliminating the non-LTE radiation field for these transitions: the b_i then show much smaller deviations from unity, typically < 0.2 dex even close to the outer boundary of our models. The more excited levels are also affected by photoionizations but also show a stronger collisional coupling to the ground state of Mg II, resulting in smaller departures.

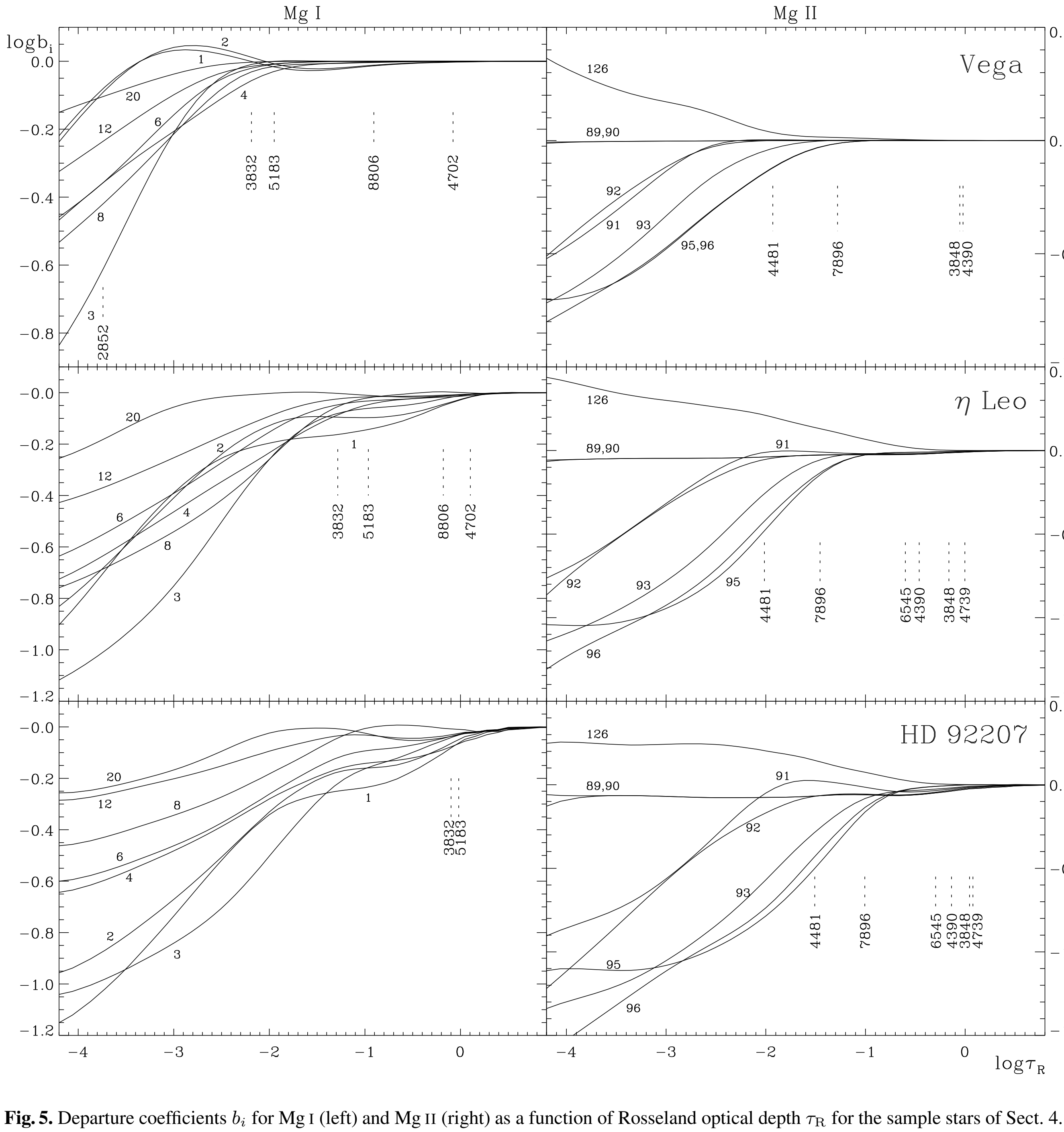

Fig. 5. Departure coefficients b_i for Mg I (left) and Mg II (right) as a function of Rosseland optical depth τ_R for the sample stars of Sect. 4. The formation depths of the line cores ($\tau \approx 1$) for several transitions are indicated. Term identifiers (also to be used with Tables 3 and 4):

1: 3s^2 ^{1}S	6: 3d ^{1}D	21: 5d ^{3}D	90: 3p ^{2}P^o	95: 4d ^{2}D	99: 5d ^{2}D	116: 8g ^{2}G
2: 3p ^{3}P^o	8: 3d ^{3}D	28: 3p^2 ^{3}P	91: 4s ^{2}S	96: 4f ^{2}F^o	106: 6g ^{2}G	126: 2p^6 ^{1}S (Mg III)
3: 3p ^{1}P^o	12: 4d ^{1}D	42: 7d ^{1}D	92: 3d ^{2}D	97: 5p ^{2}P^o	111: 7g ^{2}G	
4: 4s ^{3}S	20: 5d ^{1}D	89: 3s ^{2}S	93: 4p ^{2}P^o	98: 6s ^{2}S	115: 8f ^{2}F^o	

The lowest two energy levels of Mg II are essentially in LTE throughout the atmosphere, even for the supergiant models. Practically all radiative transitions from the ground state occur at optically thick conditions (at wavelengths shortward of the Lyman jump or coinciding with Lyman lines), thus reducing the non-LTE effects. In addition, collisions couple the first excited level to the ground state (with the collisional rates exceeding the radiative rates typically by several orders of magnitude). The optically thick resonance lines in the UV (Mg II $\lambda\lambda$ 2795,2802) are therefore in detailed balance throughout the depth range of our models (but see also Sect. 4.4).

Photoionizations help to depopulate the lower excited Mg II levels (mostly the 3d and the $n = 4$ levels) and facilitate the overpopulation of the Mg III ground state. Adopting B_ν for the

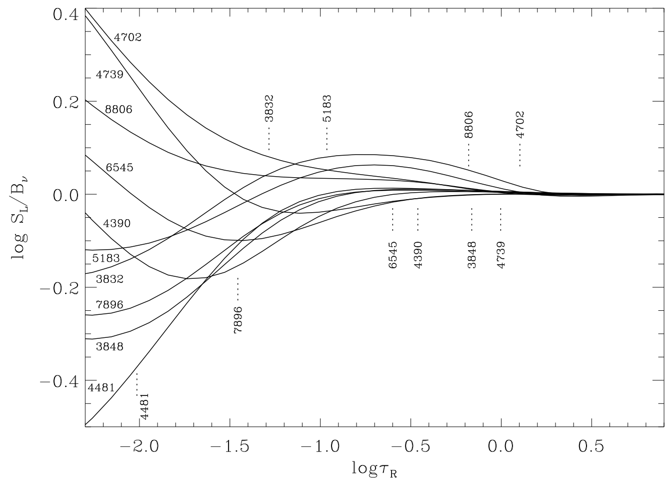

Fig. 6. Ratio of line source function $S_{\rm L}$ to Planck function B_ν at line centre for diagnostic Mg I/II lines as a function of $\tau_{\rm R}$ for our model of η Leo. The formation depths of the line cores ($\tau_{\rm R} \approx 1$) are indicated.

photoionization continua of the Mg II levels in the case of our η Leo model (see above) results in a slight underpopulation of Mg III instead. In addition, the 3d and 4s levels are kept close to LTE populations throughout the line formation region due to their (optically thick) radiative coupling with the thermalised 3p level. Then, the depopulation of the other Mg II levels results from the complex interaction of photoionizations, collisional ionizations *and* excitation processes. Modifications in the ionizations via photon or electron impact (by setting $J_\nu = B_\nu$ or increasing the b-f collision rates of the highly excited Mg II levels ($n \geq 8$) by a factor of thousand) alone do not remove these strong depopulations; they are only weakened. Again, the highly excited levels of Mg II approach the departure of the ground state of the higher ionization stage.

The non-LTE abundance corrections for our sample stars as derived in Table 3 are explained in view of the run of the departure coefficients and the corresponding line source function $S_{\rm L}$ for a given transition. Fig. 6 shows the ratio of the line source function to the Planck function

$$\frac{S_{\rm L}}{B_\nu} = \frac{\exp(h\nu_{ij}/kT) - 1}{n_i g_j / n_j g_i - 1} = \frac{\exp(h\nu_{ij}/kT) - 1}{b_i/b_j \exp(h\nu_{ij}/kT) - 1} \qquad (3)$$

for diagnostic lines in our model for the supergiant η Leo. h denotes the Planck constant, ν_{ij} the transition frequency, k the Boltzmann constant, T the temperature, n the occupation numbers and g the statistical weights of the lower/upper level i/j. The behaviour of $S_{\rm L}/B_\nu$ is qualitatively the same for the other two objects, but the deviations from the Planck function are much smaller in Vega and even stronger for the case of HD 92207.

A non-LTE strengthening of lines will occur in cases where $b_i > b_j$; otherwise a weakening is seen, as is inferred from Eqn. 3. Thus, the entirely positive non-LTE corrections for Mg I transitions in the supergiants result from the relative overpopulation of the upper levels, leading to shallower line profiles ($S_{\rm L}/B_\nu > 1$). The triplet lines in Vega, on the other hand, experience a strengthening as the line cores are formed farther out in the atmosphere where the ratio of $S_{\rm L}$ to B_ν drops below unity. For the singlet lines the conditions are similar to those of the supergiant case. In Mg II only the features $\lambda\lambda$ 4481 and 7877-96 are affected by stronger non-LTE corrections, as can be inferred from the formation depths ($\tau \approx 1$) of the corresponding line cores as marked in Figs. 5 and 6. Photon escape most probably reduces the line centre intensities of these lines, an effect strongest in the extended atmospheres of supergiants. For the other Mg II lines the ratio $S_{\rm L}/B_\nu$ remains close to unity.

3.2. Microturbulence

Microturbulence was introduced as a parameter to bring model calculations into better agreement with observation. The concept of some additional non-thermal line-broadening is not physically excluded, despite the lack of a comprehensive theoretical explanation for it at present.

Recently, McErlean et al. (1998) explicitly included microturbulence in the statistical-equilibrium calculations (with DETAIL, Eqn. 1) for helium in OB stars and find significantly different profiles as compared to the standard procedure of including microturbulence only in the final step of the spectrum synthesis (with SURFACE) for microturbulent velocities in excess of 10 km s^{-1}.

This rather subtle effect depends on the details of the ionization balance and the departure coefficients for a given element as shown by Przybilla et al. (2000). Lines from both species, Mg I and Mg II, are expected to show some sensitivity to a non-zero microturbulence in the statistical-equilibrium calculations as the occupation numbers of the levels involved vary significantly over the line-formation depths. Thus the radiative transitions occur under slightly different conditions as the formation depths of the line centres are pushed deeper into the atmosphere but simultaneously the frequency bandwidths for absorption are broadened by an increased microturbulent velocity. Changes in the non-LTE level populations and the line source functions vary in magnitude for different lines. Even lines too weak to react sensitively to microturbulence in the classical sense might therefore be affected.

In Fig. 7, test calculations for our model of η Leo with an increased microturbulence are displayed. For the weak Mg I λ 8806 feature, the equivalent width decreases by $\sim$20% as ξ is increased from 0 to 10 km s^{-1} in the statistical-equilibrium computations with DETAIL. The line formation is then performed with SURFACE on the basis of the resulting population numbers for $\xi = 10$ km s^{-1}, as in the classical approach. Equivalent widths for all other Mg I lines are also decreased with variations of typically several percent. On the other hand, Mg II lines are strengthened by several percent ($\sim$12% at maximum).

For typical microturbulence values (< 10 km s^{-1}) found in our sample stars, the magnitude of this effect is reduced but nevertheless has to be accounted for in high S/N observations such as ours. Moreover, the systematical weakening of Mg I and strengthening of Mg II lines mimics a change in effective temperature – impacting all other derived quantities. We therefore use a consistent microturbulence in all our statistical-equilibrium and line-formation calculations in order to reduce

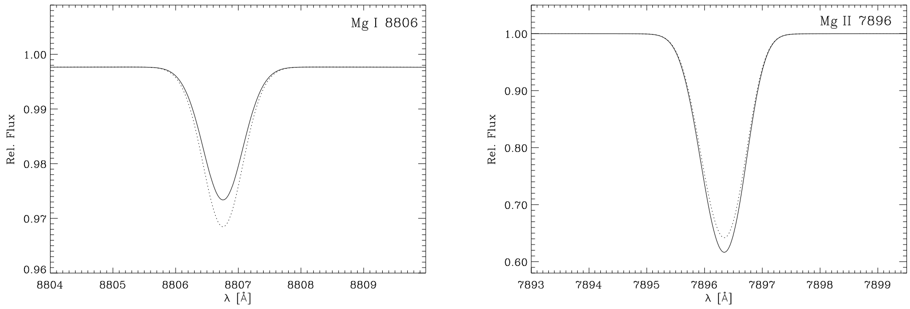

Fig. 7. Theoretical line profiles for the η Leo model (Sect. 4) with an increased microturbulence of $\xi = 10\,\mathrm{km\,s^{-1}}$. Solid line: statistical-equilibrium calculation with microturbulence included (Eqn. 1); dotted line: without microturbulence.

the systematic error in the stellar parameter and abundance determination.

3.3. Pressure inversion in atmospheric models and its implication on stellar parameter determinations

Pressure inversion is an uncommon phenomenon encountered in atmospheric modeling. It develops in hydrostatic equilibrium models for cases where the stellar luminosity *locally* exceeds the Eddington luminosity, resulting in

$$\frac{\mathrm{d}P_{\mathrm{gas}}}{\mathrm{d}r} = -\rho g + \frac{1}{c}\int_0^\infty \kappa_\nu \mathcal{F}_\nu \mathrm{d}\nu > 0. \tag{4}$$

Here P_{gas} denotes the gas pressure, ρ the density, g the surface gravity, κ_ν the total mass extinction coefficient, $\mathcal{F}_\nu$ the flux, c the speed of light and r the radial coordinate. Supergiant models at $T_{\mathrm{eff}} \lesssim 8000\,\mathrm{K}$ are susceptible to the development of pressure inversion due to their intrinsic low surface gravity and a strong peak in opacity as hydrogen ionizes in the low density regions of the photosphere.

A pressure inversion layer can also be present in hydrodynamical models where Eqn. 4 has to be replaced by the momentum equation as Achmad et al. (1997) and Asplund (1998) have shown. It is not removed by mass outflow except for very high mass loss rates not supported by the observations. Moreover, this local super-Eddington luminosity does not initiate the stellar wind. In a stability analysis for late-type stars close to the Eddington limit, Asplund (1998) finds no conclusive evidence for the suppression or the realization of pressure inversion in real stellar atmospheres. Further efforts with more sophisticated methods are needed.

Nevertheless, assuming that the pressure inversion is an artefact of inappropriate assumptions in the model atmosphere calculations, the determination of stellar parameters on the basis of these models becomes subject to systematic uncertainties which are hard to quantify. In particular, supergiant models with T_{eff} between 7000 K and 8000 K (corresponding to late A-type and early F-type) will be affected as the pressure inversion layer extends into the line-forming region (see Table 1 in Achmad et al. 1997). At cooler temperatures, the hydrogen ionization zone progressively shifts to deeper atmospheric layers and the modeling of spectral features will be only influenced indirectly.

In our approach the surface gravity is determined by Balmer line fitting. The shape of the hydrogen lines is determined by (linear) Stark broadening which reacts sensitively to the local electron density ($\propto n_{\mathrm{e}}$). Within a pressure inversion layer this density is increased by up to an order of magnitude in some cases. The derived surface gravities will therefore be systematically underestimated. Also, the temperature indicator – the Mg I/II ionization equilibrium – is affected, even if to a lesser extent. In the simplified case of LTE the local electron density influences the ionization balance through the Saha equation. Higher electron densities result in a strengthening of the calculated Mg I line strengths. An overestimation of T_{eff} will follow from a comparison with the observations. This situation also arises in non-LTE, at least qualitatively.

The suspected higher $\log g$ values help to resolve discrepancies in the mass determination for these objects. Spectroscopic masses are in better agreement with the masses determined from evolutionary tracks for higher surface gravities at a given luminosity.

On the other hand, it should be noted that the determination of elemental abundances seems not to be severely affected by these systematics on the parameter analysis and the enhanced (metal) line broadening (quadratic Stark and van der Waals damping) due to higher particle densities. Objects for "critical" combinations of $T_{\mathrm{eff}}/\log g$ show similar abundances as objects well outside the pressure inversion regime (see e.g. Venn 1995). The question of whether this is a coincidence or evidence for realization of pressure inversion in real stellar atmospheres can be settled by an analysis of an appropriate (visual) binary system with one component in the pressure inversion regime and the other outside, which would act as the abundance reference. This test still has to be performed.

From these considerations, some doubt in the reliability of present modeling techniques for late A-type and F-type supergiants seems appropriate. We therefore refrain from including such stars in our sample in Sect. 4 which would otherwise extend the variety of diagnostic lines for Mg I/II. A quantitative analysis of the problem is far beyond the scope of this work but we hope to have given further motivation to study this sparsely-populated region of the Hertzsprung-Russell diagram (e.g. Blaha & Humphreys 1989).

3.4. Comparison with other studies

So far, the only Mg I/II non-LTE model atom comparable to ours in complexity is that of Gigas (1988). A comparison of both is desireable in order to check the validity of the non-LTE calculations.

Gigas himself performs non-LTE calculations for magnesium only for Vega. The departure coefficients found by him (Fig. 3 and 4 in Gigas 1988) show qualitatively and quantitatively similar behaviour to ours (Fig. 5). Consequently, as the atmospheric parameters and gf values do not differ drastically, his LTE and non-LTE abundances match well with ours within the uncertainties (see Table 5). Nevertheless, some trend seems to be indicated: the Mg b lines and the Mg II λ4481 feature are subject to stronger non-LTE corrections in our approach.

The systematic differences are expected to be amplified in supergiants at conditions more suitable for non-LTE. Venn (1995) analyses the supergiant η Leo using the Gigas model to determine the magnesium ionization equilibrium. Indeed, our abundance corrections for the Mg I lines are more pronounced, by over 0.1 dex, whereas those for the weak Mg II lines show no significant differences. Accounting for her higher $T_{\rm eff}$ value for this star even worsens the situation, as the difference in the non-LTE abundance corrections increases.

Our consistent modeling of the observations for Vega and η Leo with reduced random errors (cf. Table 5) clearly indicates the improvement achieved in the description of the real processes, applying our model atom instead of that of Gigas (1988). The recent efforts of various groups in providing accurate atomic data play an important part in this.

4. Application to observations

4.1. The spectra

As a test and first application of the model atom, the atmospheric parameters and magnesium abundances for three objects are determined: the main sequence star Vega (HD 172167), the supergiant η Leo (HD 87737) and the object HD 92207, close to the Eddington limit. High S/N and high resolution spectra are used in this process.

For both supergiants, Echelle spectra using FEROS (Kaufer et al. 1999) at the ESO 1.52m telescope in La Silla were taken in January 1999. Nearly complete wavelength coverage between 3600 and 9100 Å was achieved with a resolving power $R = \lambda/\Delta\lambda \approx 48000$ (with 2.2 pixels per $\Delta\lambda$ resolution element) yielding a S/N of several hundred in V. The exposure times were 2 min (η Leo) and 5 min (HD 92207). Data reduction was performed using the MIDAS package, as described in the FEROS documentation (http://www.ls.eso.org/lasilla/Telescopes/2p2T/E1p5M/FEROS/docu/Ferosdocu.html). The spectra were normalized by fitting a spline function to continuum points and finally shifted in wavelength to the rest frame using the radial velocity $v_{\rm rad}$ determined from cross-correlation with an appropriate synthetic spectrum.

An Echelle spectrum of Vega was kindly made available by A. Korn with almost complete wavelength coverage between 3900 and 9400 Å. FOCES (Pfeiffer et al. 1998) at the Calar Alto 2.2m telescope was used in June 1999 to obtain three exposures of 4 s and 2×10 s, respectively. The spectra were reduced in the standard way using the routines described by Pfeiffer et al. (1998). After merging of the single spectra and rectification, a S/N of $\sim$750 near H_α was measured at $R \approx 40000$ (2 pixels per $\Delta\lambda$ resolution element).

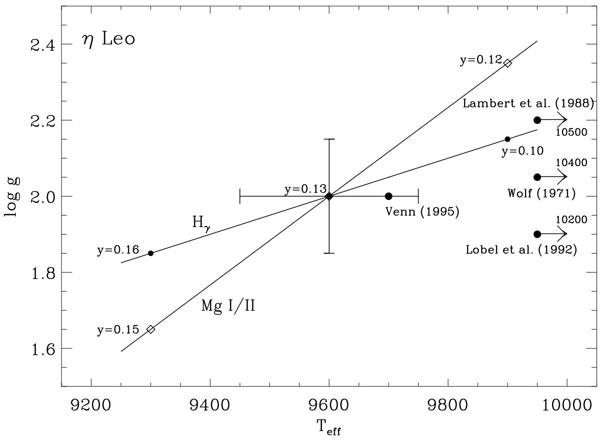

Fig. 8. H_γ and Mg I/II loci for η Leo on the temperature-gravity plane with the helium abundance y as an additional parameter. The adopted values for $T_{\rm eff}$/log g are shown with their estimated uncertainties. Atmospheric parameters used in other analyses are also displayed: arrows indicate shifts in $T_{\rm eff}$ to the values cited.

A second spectrum of Vega taken with HEROS was provided by A. Kaufer, extending the wavelength range for the analysis from 3900 Å down to the Balmer jump. A S/N>200 at $R \approx 20000$ was achieved (cf. Kaufer et al. (1996a, 1996b) for details on the observations and the data reduction procedures).

In general, the observations are of high quality with few spectral regions corrupted by CCD defects or cosmic ray impacts. As the data were obtained only as a supplement to the main observing program, no additional spectra of a fast rotator are available at the correct airmass to remove the telluric features.

4.2. Determination of the atmospheric parameters

Prior to an abundance analysis, atmospheric parameters have to be determined accurately. A purely spectroscopic approach is chosen. $T_{\rm eff}$ and $\log g$ are derived simultaneously by finding the ionization equilibrium of Mg I/ II and by fitting the wings of the higher Balmer lines (typically from H_γ upwards) which are still formed in photospheric regions, in contrast to the H_α and H_β features which are affected by the stellar wind in supergiants. The profiles are calculated using the Stark broadening tables of Vidal et al. (1973). He I lines are used to assess the stellar helium abundance $y = n({\rm He})/[n({\rm H}) + n({\rm He})]$. The stellar density structure responds to changes in the helium abundance because of its higher mean molecular weight (see e.g. Kudritzki 1973). $T_{\rm eff}$ and $\log g$ have to be appropriately adjusted at this point in some cases, see Fig. 8. The microturbulent velocity ξ is determined from LTE spectrum synthesis for a large ensemble of Fe II and Cr II lines by demanding that there is no relation between abundance and line strength. From this, the metallicity of the object is also fixed by assuming [M/H]=[Fe/H]. Elemental abundances for the important background-opacity species are obtained by detailed non-LTE

Table 2. Basic properties and atmospheric parameters for the test stars

HD	Name	Sp. Type	V (mag)	l (°)	b (°)	$v_{\rm rad}$ (km s^{-1})	$v \sin i$ (km s^{-1})	$T_{\rm eff}$ (K)	log g (cgs)	y	ξ (km s^{-1})	$\zeta_{\rm RT}$ (km s^{-1})
172167	α Lyr, Vega	A0 V	0.03	67.44	+19.24	−14	22	9550	3.95	0.09	2	0
							±2	±150	±0.1	±0.01	±0.5	+2
87737	η Leo	A0 Ib	3.52	219.53	+50.75	+3	9	9600	2.00	0.13	4	12
							±1	±150	±0.15	±0.02	±1	±2
92207	…	A0 Iae	5.45	286.29	−0.26	−9	28	9100	0.98	0.23	6	18
							±4	$^{+400}_{-150}$	$^{+0.30}_{-0.15}$	$^{+0.03}_{-0.10}$	±2	±4

Table 3. Abundance analysis for magnesium in the test stars

						α Lyr			η Leo			HD 92207		
λ (Å)	χ (eV)	Trans.	log gf	Acc.	Source	W_λ(mÅ)	log ε	Δ log ε	W_λ(mÅ)	log ε	Δ log ε	W_λ(mÅ)	log ε	Δ log ε
Mg I:														
3829.36	2.71	2−8	−0.21	B	NIST	S	7.07	−0.08	S	7.49	+0.14	S	7.31	+0.18
3832.30	2.71	2−8	0.27	B	NIST	S	7.05	−0.31	S	7.41	+0.19	S	7.28	+0.30
3838.29	2.72	2−8	0.49	B	NIST	…	…	…	S	7.44	+0.14	S	7.31	+0.29
4167.27	4.35	3−42	−1.71	C+	OP	20	7.04	+0.00	…	…	…	…	…	…
4702.99	4.35	3−20	−0.42	C+	OP	31	6.96	+0.02	12	7.64	+0.14	…	…	…
5167.32	2.71	2−4	−0.86	B	NIST	…	…	…	…	…	…	…	…	…
5172.68	2.71	2−4	−0.38	B	NIST	S	7.04	−0.06	S	7.53	+0.15	S	7.28	+0.17
5183.60	2.72	2−4	−0.16	B	NIST	125	7.04	−0.13	90	7.51	+0.12	23	7.25	+0.18
5528.41	4.35	3−12	−0.40	C+	OP	28	6.91	+0.03	6	7.60	+0.17	…	…	…
8806.76	4.35	3−6	−0.16	C+	OP	S(62)	7.06	−0.03	…	…	…	…	…	…
Mean							7.02	7.09		7.52	7.37		7.29	7.06
σ							0.06	0.15		0.08	0.10		0.03	0.06
Mg II:														
3848.21	8.86	92−97	−1.49	C	OP	S(8)	7.05	+0.00	S(59)	7.52	+0.05	31	7.26	+0.05
3848.34	8.86	92−97	−2.40	D	OP									
3850.39	8.86	92−97	−1.74	C	OP	…	…	…	S	7.54	+0.05	S	7.28	+0.03
4384.64	10.00	93−99	−0.79	C+	NIST	…	…	…	S	7.54	−0.02	…	…	…
4390.51	10.00	93−99	−1.70	C+	NIST	S(28)	6.98	+0.00	95	7.54	−0.02	52	7.26	+0.03
4390.57	10.00	93−99	−0.53	C+	NIST									
4427.99	10.00	93−98	−1.20	C+	NIST	7	7.03	+0.00	32	7.56	+0.02	…	…	…
4433.99	10.00	93−98	−0.90	C+	NIST	12	7.02	+0.00	49	7.55	+0.02	…	…	…
4481.13	8.86	92−96	0.73	B	NIST									
4481.15	8.86	92−96	−0.57	B	NIST	S(310)	6.99	*−0.21*	…	…	…	636	7.23	*−0.88*
4481.33	8.86	92−96	0.57	B	NIST									
4739.59	11.57	95−115	−0.66	C+	OP	…	…	…	33	7.50	+0.01	9	7.23	+0.03
4739.71	11.57	95−115	−0.77	C+	OP									
4851.08	11.63	96−116	−0.42	C	CA	…	…	…	S(24)	7.51	+0.02	S(10)	7.33	−0.03
5401.54	11.63	96−111	−0.08	C	CA	…	…	…	S	7.57	−0.03	…	…	…
6545.97	11.63	96−106	0.41	C	CA	…	…	…	S(75)	7.61	−0.11	S(56)	7.28	−0.16
7877.05	10.00	93−95	0.39	C+	NIST	…	…	…	S	7.45	*−0.43*	…	…	…
7896.04	10.00	93−95	−0.30	C+	NIST	…	…	…	S	7.48	*−0.49*	…	…	…
7896.37	10.00	93−95	0.65	C+	NIST									
Mean						7.01	7.02		7.53	7.55		7.27	7.28	
σ						0.03	0.03		0.04	0.07		0.03	0.10	
Mg I/II						7.02	…		7.53	…		7.28	…	
σ						0.05	…		0.06	…		0.03	…	

Term identifiers for the transitions are specified in the caption of Fig. 5. Sources of the gf values: CA: calculated from the Coulomb approximation (Bates & Damgaard 1949); NIST: Fuhr & Wiese (1998) as available electronically from the NIST 2.0 database; OP: Opacity Project data, Butler et al. (1993) for Mg I and K.T. Taylor (available only electronically from the TOPBASE database) for Mg II. Accuracy indicators: B: 10%, C: 25%, D: 50%. Entries in *italics* are not used in the determination of means and standard deviations.

calculations (see Sect. 2.3). Rotational velocities $v \sin i$ and macroturbulence $\zeta_{\rm RT}$ in the radial-tangential model are derived from spectrum synthesis as both broadening mechanisms alter the line profile in different ways (Gray 1992). Usually, several iteration steps are necessary to obtain the final set of parameters.

The basic properties and atmospheric parameters of the test stars are summarised in Table 2, as are the error estimates. Information on the basic properties are taken from the Bright Star Catalogue (Hoffleit 1982).

The atmospheric model for our spectrum synthesis calculations on Vega is adopted from Castelli & Kurucz (1994). Excellent agreement between observations and our spectrum synthesis is found on the basis of this model, thus confirming the reliability of the atmospheric parameters derived in that work.

4.3. Abundance analysis

The results of the abundance analysis for magnesium are summarised in Table 3 which gives the wavelength, lower excitation potential, energy levels involved in the transition (see the caption of Fig. 5 for term identifiers) and the adopted gf value for the observed lines, with accuracy indicators and sources for the gf values. Measured equivalent widths, derived abundances

$$\log \varepsilon = \log({\rm Mg/H}) + 12 \quad (5)$$

and non-LTE abundance corrections

$$\Delta \log \varepsilon = \log \varepsilon_{\rm NLTE} - \log \varepsilon_{\rm LTE} \quad (6)$$

for the different stars are also displayed. Blended lines are marked by "S" as long as an analysis via spectrum synthesis is still feasible and for lines originating in the hydrogen line wings the equivalent widths are measured against the local continuum (W_λ in parentheses). Non-LTE and LTE mean values and the line-to-line scatter (σ) are displayed, as is the combined abundance from Mg I/II in the non-LTE case. Note that the abundances are derived from the detailed spectrum synthesis results and not from an equivalent-width study.

In Fig. 9, theoretical line profiles for the derived mean non-LTE magnesium abundance are compared with the observations; excellent agreement is found with few exceptions (Mg I $\lambda\lambda$ 4702 and 5528). For comparison, profiles from the mean LTE abundance (Mg II) are also shown. Other elements are included for the spectrum synthesis in LTE in order to disentangle line blends. As some of the magnesium lines are formed in the wings of H I lines, profiles for hydrogen are calculated on the basis of non-LTE level populations. He I is also treated in non-LTE due to its importance for the atmospheric structure. The magnesium abundances for the test stars are:

Vega	$\log({\rm Mg/H}) + 12 = 7.02 \pm 0.05 \pm 0.05$ (13)
η Leo	$\log({\rm Mg/H}) + 12 = 7.53 \pm 0.06 \pm 0.10$ (19)
HD 92207	$\log({\rm Mg/H}) + 12 = 7.28 \pm 0.03 \pm 0.15$ (12)

We list the values obtained from the non-LTE analysis together with uncertainties from the line-to-line scatter and systematic errors (cf. Sect. 2.4); the number of analysed lines is given in parentheses. Non-LTE shifts the derived Mg I abundances systematically to higher and the Mg II abundances to lower values and the line-to-line scatter is reduced in comparison to LTE.

Vega shows a magnesium deficiency of 0.56 dex. This is comparable to the general underabundance of the heavier elements by typically $\sim$0.5 dex (solar abundances adopted from Grevesse et al. 1996) which leads to the conclusion that Vega is a mild λ Bootis star (Venn & Lambert 1990). We find only small non-LTE corrections for this main sequence star. In the case of η Leo the magnesium abundance is consistent with the solar value, as are the abundances of other α and iron peak elements. Non-LTE corrections are <0.2 dex for most of the lines. These corrections slightly increase at still higher luminosity, as for HD 92207. For this star we derive [Mg/H]=-0.3 dex which matches well with its elemental underabundance of $\sim$0.4 dex. As discussed earlier, non-LTE effects on the atmospheric structure of this extreme object are expected which would bring its metal abundance into better agreement with typical abundances derived for galactic objects.

Table 4. Atomic data for UV line formation in Vega

λ (Å)	χ (eV)	Trans.	$\log gf$	Acc.	Source
Mg I:					
2776.690	2.71	2–28	−0.121	C	NIST
2778.271	2.71	2–28	−0.214	C	NIST
2779.820	2.71	2–28	−0.341	C	NIST
2779.834	2.72	2–28	0.356	C+	NIST
2781.416	2.71	2–28	−0.211	C	NIST
2782.971	2.72	2–28	−0.123	C	NIST
2846.717	2.71	2–21	−1.262	D−	NIST
2848.344	2.71	2–21	−1.396	D−	NIST
2848.346	2.71	2–21	−0.894	D−	NIST
2851.652	2.72	2–21	−2.556	E	NIST
2851.654	2.72	2–21	−1.382	D−	NIST
2851.656	2.72	2–21	−0.637	D−	NIST
2852.126	0.00	1–3	0.258	B	NIST
Mg II:					
2790.777	4.42	90–92	0.272	C	NIST
2795.528	0.00	89–90	0.086	C	NIST
2797.930	4.43	90–92	−0.431	B	NIST
2797.998	4.43	90–92	0.529	C	NIST
2802.705	0.00	89–90	−0.213	C	NIST
2928.633	4.42	90–91	−0.510	C	NIST
2936.510	4.43	90–91	−0.225	C	NIST

See Table 3 for accuracy indicators and gf value sources.

4.4. Magnesium lines in the UV

An additional check for the reliability of our model atom is provided by the results from modeling several strategic UV lines of Mg I/II. We perform this test for Vega only as we are mainly interested in the behaviour of the resonance lines which are already affected by contamination of interstellar absorption for this nearby star; see e.g. Lallement et al. (1995) or Kondo et al. (1978). Also, excellent observational material of the spectral region of interest is available for this object only. We use the high S/N, high resolution spectral atlas obtained with the

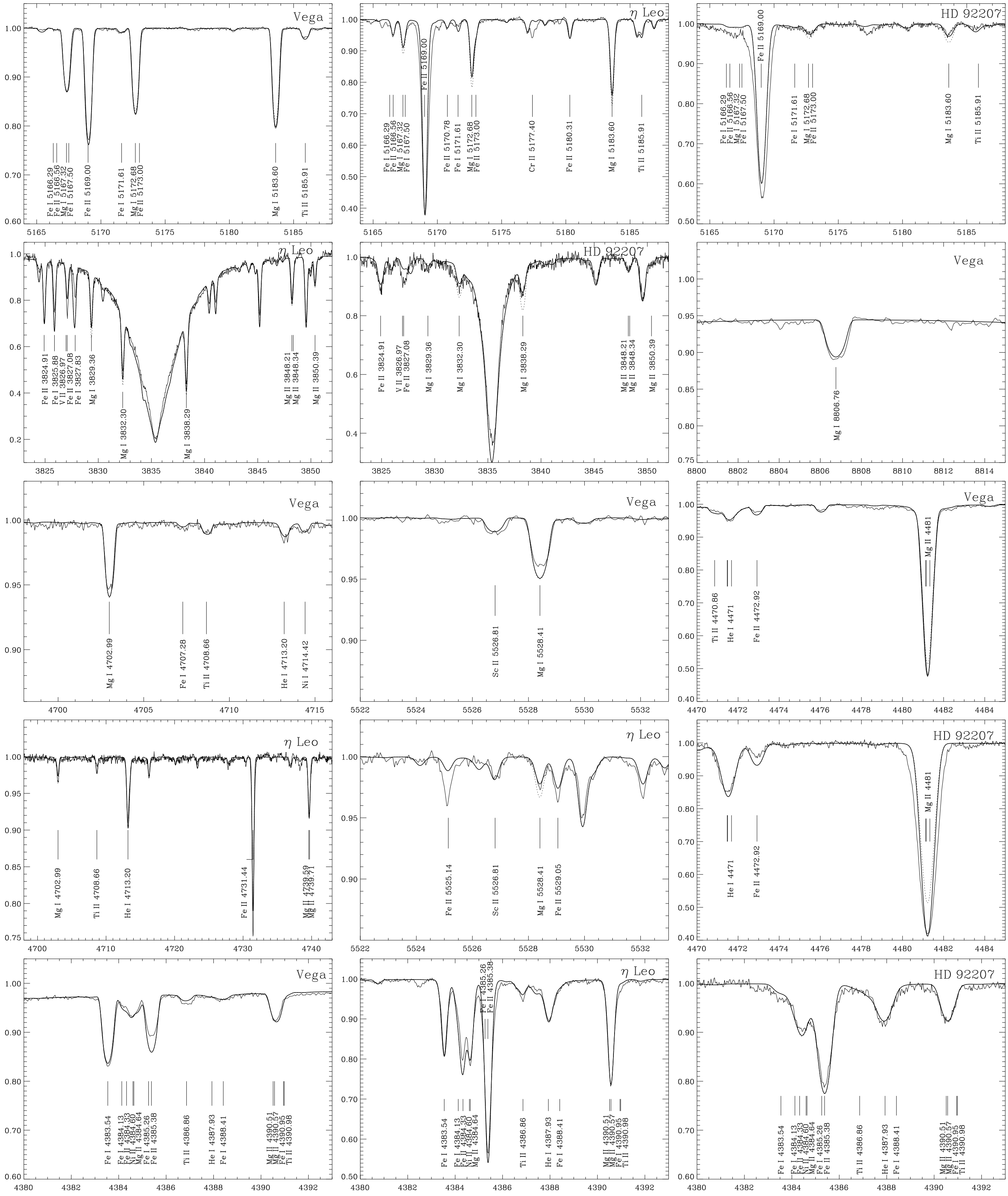

Fig. 9. Spectral synthesis for selected Mg I/II lines in the test stars. Abscissa units are wavelengths in Å, ordinate is relative flux. Observed (thin solid) and computed (thick solid) non-LTE profiles for the magnesium abundances in Table 3 are displayed with line identifiers. Profiles for the appropriate Mg II LTE abundances are marked by a dotted line. Line formation for species other than H I, He I and Mg I/II is performed assuming LTE level populations. Note that in the case of Mg I λ8806 the local continuum for Vega is determined by overlapping Paschen lines.

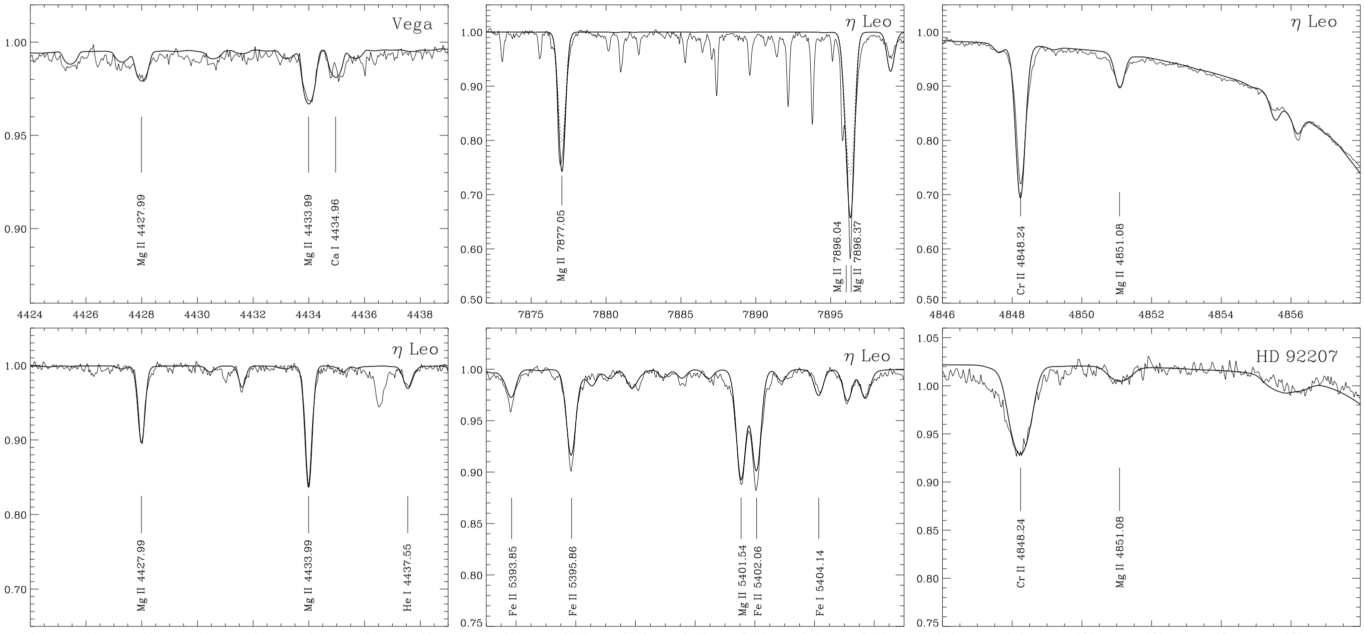

Fig. 9. (cont) Numerous sharp telluric lines contaminate the red part of the spectrum. Note that the local continuum in the wing of H_β is enhanced by incoherent electron scattering (see McCarthy et al. 1997) for a discussion of this effect); our result for the hydrostatic calculation has been shifted to compensate for this at least partially.

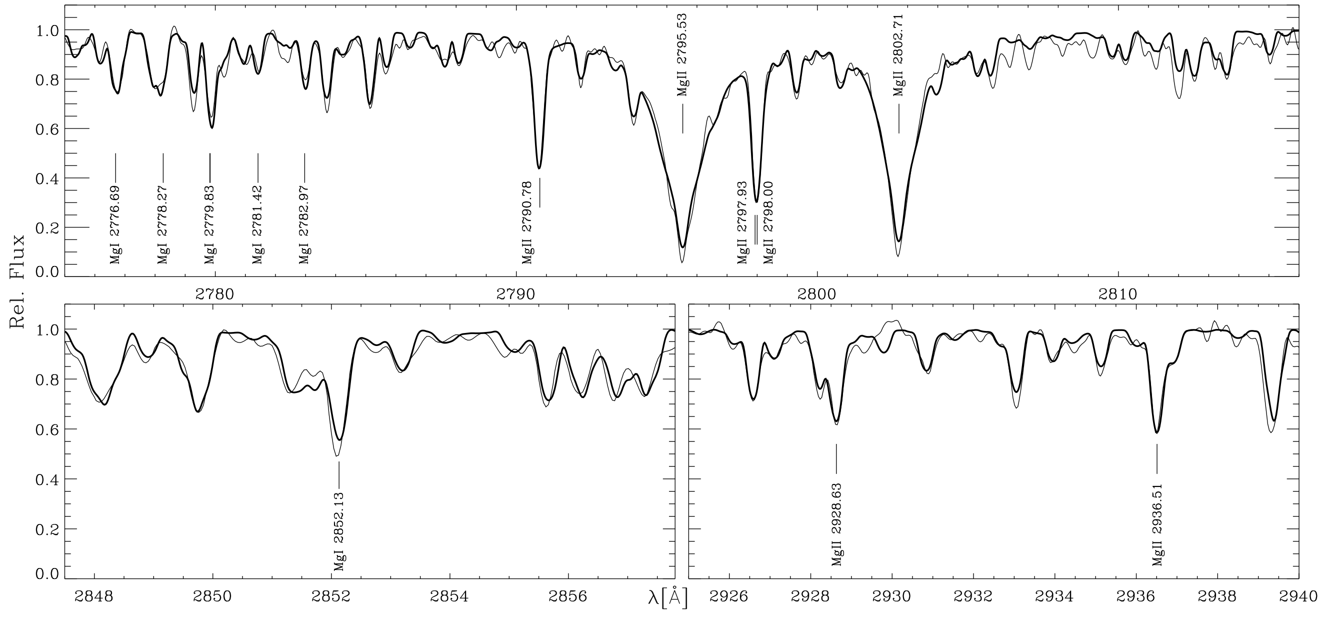

Fig. 10. Spectral synthesis of the UV region in Vega. Observed (thin solid) and computed (thick solid) non-LTE profiles (for $\log \varepsilon(\mathrm{Mg})=7.02$) are displayed with Mg I/II line identifiers. See text for details on the possible interstellar contamination of the resonance line centres.

COPERNICUS satellite (Rogerson 1989). For the other stars (at larger distances), the interstellar components will severely blend the stellar lines. Moreover, at high luminosities these lines become stellar-wind dominated, which cannot be modelled in our approach.

Spectrum synthesis is mandatory for the interpretation of the UV lines in Vega. In addition to magnesium we include the iron peak elements in our line-formation calculation which account for the overwhelming majority of lines in the spectral region of interest. The gf values are adopted from Kurucz & Bell (1995) or from Martin et al. (1988) and Fuhr et al. (1988) where available. Elemental abundances are adopted from previous determinations from lines in the visual. The atomic data for the magnesium lines are summarised in Table 4. Fitting of the observed resonance line profiles is best accomplished by using collisional damping data calculated from the approximation of Cowley (1971).

There is generally good accordance between observations and our model calculations; see Fig. 10. The discrepancies are expected to arise from observational noise, inaccurate atomic

Table 5. Comparison of Mg I/II abundances for α Lyr and η Leo

Source	$\log \varepsilon_{\rm LTE}(\rm Mg\,I)$	$\log \varepsilon_{\rm LTE}(\rm Mg\,II)$	$\log \varepsilon_{\rm NLTE}(\rm Mg\,I)$	$\log \varepsilon_{\rm NLTE}(\rm Mg\,II)$
		α Lyr		
This work	7.09 ± 0.15 (8)	7.02 ± 0.03 (4)	7.02 ± 0.06 (8)	7.01 ± 0.03 (5)
Castelli (1993)	7.04	7.04	...	...
Venn & Lambert (1990)	...	6.71 ± 0.16 (3)	...	...
Adelman & Gulliver (1990)	6.93 (1)	6.89 ± 0.05 (5)	...	...
Gigas (1988)	7.07 ± 0.10 (5)	6.96 ± 0.10 (3)	7.08 ± 0.08 (5)	6.92 ± 0.09 (3)
Freire Ferrero et al. (1983)	...	...	...	7.00 (2)
Sadakane & Nishimura (1981)	7.53 (1)	...	...	...
Sadakane & Nishimura (1979)	7.39 ± 0.17 (2)	7.04 (1)	...	...
		η Leo		
This Work	7.37 ± 0.10 (7)	7.55 ± 0.07 (10)	7.52 ± 0.08 (7)	7.53 ± 0.04 (11)
Venn (1995)	7.55 ± 0.12 (4)	7.54 ± 0.14 (5)	7.58 (4)	7.46 (5)
Lambert et al. (1988)	...	7.78	...	...
Wolf (1971)	7.76 (1)	7.84 ± 0.11 (6)	...	...

listed are the abundances with 1σ errors from the line-to-line scatter (number of lines analysed in parenthesis)

data, unaccounted line blends by other elements and neglected non-LTE effects for the iron group elements. In particular, the majority of the magnesium lines are correctly predicted except for the centres of the resonance lines. Here interstellar absorption is likely to contribute to the observed line profiles. The extra absorption slightly blueward of the line centres of Mg I λ 2852 and Mg II $\lambda\lambda$ 2795-2802 is well correlated with the interstellar Fe II components identified by Lallement et al. (1995). In addition the Mg II resonance lines remain optically thick even at the outer boundary of our model atmosphere, at $\log \tau_{\rm R} = -8$. The centres of these lines are therefore artifically truncated, introducing a small inaccuracy. In general, deviations from LTE are small for the UV magnesium lines.

4.5. Comparison with other analyses

In the following, our results for the sample stars are compared with those of other recent analyses.

Vega Vega is an important photometric standard and has therefore been the subject of several abundance studies. Castelli (1993) derives a LTE abundance from the UV lines of Mg I/II. The model atmosphere used is almost identical to ours, which results in a magnesium abundance consistent with our findings.

Venn & Lambert (1990) find a magnesium abundance 0.35 dex lower than our value from an LTE analysis of Mg II λ 4481 and two IR lines not included in our study. Atmospheric parameters of $T_{\rm eff} = 9650$ K and $\log g = 4.0$ have been used with ATLAS6 (Kurucz 1979) and gf values identical with ours (in the case of Mg II λ 4481). The discrepancy most likely results from the broadening data used in the line-formation calculations as the measured equivalent widths only differ by several percent.

Adelman & Gulliver (1990) derive a slightly lower LTE magnesium abundance from almost identical equivalent widths and gf values as used in our work. A systematic shift results from their choice of atmospheric parameters (9400/3.95). Considering this, both LTE results match well.

A LTE and non-LTE study of Gigas (1988) finds Mg I/II abundances similar to ours. The small differences can be attibuted to an interplay of model parameters (9500/3.90), small variations in the measured W_λ and the choice of gf values. Our results also agree well with those of the non-LTE study by Freire Ferrero et al. (1983) of the Mg II UV resonance lines, which nevertheless are poor abundance indicators due to their saturation.

Sadakane & Nishimura (1979, 1981) find a large scatter in magnesium abundances from lines in the visible and near UV, respectively. The quality of atomic data has significantly improved in the past twenty years and their relatively high magnesium abundance (from Mg I) can, for the most part, be attributed to the inaccuracies in their gf values. Their atmospheric parameters (9660/3.94) and equivalent widths are comparable with the "modern" values.

η Leo This A0 Ib standard star has also been a target for detailed abundance studies. Venn (1995) finds LTE and non-LTE abundances – using the model atom of Gigas (1988) – consistent with our results. The stellar parameters (9700/2.0), equivalent widths and gf values used in her analysis are close to ours. Two of the Mg I lines are blends, which might explain the higher abundance of neutral magnesium in her work.

Lambert et al. (1988) find a magnesium abundance of $+0.2$ dex above solar. They do not give enough details to reconstruct their work, but the higher abundance should result from a rather high $T_{\rm eff}$ of 10500 K.

Finally the early work of Wolf (1971) found a similarly high abundance to that of Lambert et al. (1988). This results from similar stellar parameters (10400/2.05, no line blanketing) and slightly larger W_λ than those measured in the present study.

HD 92207 For this supergiant, information is scarce in the literature. Groth et al. (1990) performed a preliminary analysis on the basis of an unblanketed H-He non-LTE atmosphere.

Their stellar parameters are identical with ours except for the solar helium abundance which they derive. In their analysis, magnesium is overabundant by +0.16 dex compared to solar, which differs by almost 0.5 dex from our findings. There are not enough details provided to determine the origin of the large differences, but certainly they result from their totally different approach.

5. Summary and conclusions

An extensive model atom for non-LTE line-formation calculations for Mg I/II has been developed, based on the most accurate atomic data presently available. This allows – in combination with Balmer-line fitting – a precise determination of stellar parameters ($T_{\rm eff}/\log g$) from a purely spectroscopic approach, as the Mg I/II ionization equilibrium proves to be a highly sensitive temperature indicator. Typical uncertainties in the parameter determination amount to 150 K/0.15 dex at $T_{\rm eff} \approx 9500$ K, comparable to or even better than those of conventional (spectro)photometric methods. Moreover, our model atom allows the determination of magnesium abundances with unprecedented accuracy. The uncertainties for high quality observations amount to $\sim 0.10/0.15/0.20$ dex in early A-type stars for luminosity classes V/Ib/Ia *including* systematic errors, as confirmed by the analysis of our test stars Vega, η Leo and HD 92207. We derived the following magnesium abundances for these objects:

Vega	$\log({\rm Mg/H}) + 12 = 7.02 \pm 0.05 \pm 0.05\,(13)$
η Leo	$\log({\rm Mg/H}) + 12 = 7.53 \pm 0.06 \pm 0.10\,(19)$
HD 92207	$\log({\rm Mg/H}) + 12 = 7.28 \pm 0.03 \pm 0.15\,(12)$

Our results support the findings of a general metal underabundance of ~ 0.5 dex for Vega in previous studies. For η Leo the magnesium abundance is consistent with the solar value while in HD 92207 magnesium seems to be slightly underabundant but consideration of non-LTE effects on the atmospheric structure are likely to bring it into better concordance. Our model calculations generally match the observed profiles well. For Vega, the study of the UV spectral region containing the resonance lines further confirmes the results obtained at visual and near-IR wavelengths.

In general, non-LTE abundance corrections are small ($\lesssim 0.3$ dex) in Mg I and negligible in Mg II, except for the $\lambda\lambda$ 4481 and 7877-96 features which show marked deviations from LTE. The nature of the non-LTE effects is well understood.

Subtle effects are evoked by the inclusion of the microturbulence parameter in the statistical-equilibrium calculations for Mg I/II. In contrast to the standard approach – accounting for microturbulence only in the line formation – even weak lines might be affected by modified level populations. Mg I line strengths are systematicaly weakened while Mg II lines are strengthened, which mimics a change in the stellar effective temperature. The effect is small but cannot be neglected for high quality observations.

Finally, evidence is given that accurate analyses of late A- and early F-type supergiants are hampered by systematics originating in the pressure inversion region present in common model atmospheres. Enhanced local particle densities in the line-formation region of model atmospheres affect all broadening mechanisms and especially lead to underestimated surface gravities. No conclusive statement can be given on this topic as the question of how nature deals with this problem can only be deduced from sophisticated hydrodynamical stability analyses that still have to be performed.

Acknowledgements. We are grateful to A. Kaufer for his help with obtaining some of the spectra at La Silla and for providing observations of Vega and to S. Tubbesing for his help with the data reduction. We further express our thanks to A. Korn for providing a beautiful spectrum of Vega. We are also grateful to our referee, Dr. D. Kiselman, who helped to improve the paper by his suggestions. Funding through the MPIA, Garching, is gratefully acknowledged (NP).

References

Achmad L., Lamers H.J.G.L.M., Pasquini L., 1997, A&A, 320, 196
Adelman S.J., Gulliver A.F., 1990, ApJ, 348, 712
Allen C., 1973, Astrophysical Quantities, 3rd edn., Athlone Press, London
Asplund M., 1998, A&A, 330, 641
Bates D., Damgaard A., 1949, Phil. Trans. Roy. Soc., 242A, 101
Blaha C., Humphreys R.M., 1989, AJ, 98, 1598
Bresolin F., Kudritzki R.P., Méndez R.H., Przybilla N., 2001, ApJL, accepted
Butler K., Giddings J., 1985, Newsletter on Analysis of Astronomical Spectra No. 9, University of London
Butler K., Mendoza C., Zeippen C.J., 1990, in: Hansen J.E. (ed.), Atomic Spectra and Oscillator Strengths for Astrophysics and Fusion Research, Amsterdam: North-Holland, p. 124
Butler K., Mendoza C., Zeippen C.J., 1991, J. Physique IV, C1, 135
Butler K., Mendoza C., Zeippen C.J., 1993, J. Phys. B, 26, 4409
Carlsson M., Rutten R.J., Shchukina N.G., 1992, A&A, 253, 567
Castelli F., 1993, in: Weiss W.W., Baglin A. (eds.), Inside the Stars, San Francisco: ASP
Castelli F., Kurucz R.L., 1994, A&A, 281, 817
Chang E.S., Noyes R.W., 1983, ApJ, 275, L11
Clark R.E., Csanak G., Abdallah J., Jr., 1991, Phys. Rev. A, 44, 2874
Cowley C., 1971, Observatory, 91, 139
Crandall D.H., Phaneuf R.A., Falk R.A., et al., 1982, Phys. Rev. A, 25, 143
Cunto W., Mendoza C., 1992, Rev. Mex. Astrofis., 23, 107
Deeming T.J., 1960, MNRAS, 121, 52
Dimitrijević M.S., Sahal-Bréchot S., 1996, A&AS, 117, 127
Freire Ferrero R., Gouttebroze P., Kondo Y., 1983, A&A, 121, 59
Freund R.S., Wetzel R.C., Shul R.J., Hayes T.R., 1990, Phys. Rev. A, 41, 3575
Fuhr J.R., Martin G.A., Wiese W.L., 1988, J. Phys. & Chem. Ref. Data, Vol. 17, Suppl. 4
Fuhr J.R., Wiese W.L., 1998, in: Lide D.R. (ed.), CRC Handbook of Chemistry and Physics, 79th ed., CRC Press Inc., Boca Raton (electronically: NIST 2.0 database)
Fuhrmann K., 1998, A&A, 338, 161
Giddings J.R., 1981, Ph. D. Thesis, University of London
Gigas D., 1988, A&A, 192, 264
Gray D.F., 1992, The observation and analysis of stellar photospheres, 2nd edition, Cambridge University Press
Grevesse N., Noels A., Sauval A.J., 1996, in: Holt S.S., Sonneborn G. (eds.), Cosmic Abundances, San Francisco: ASP
Griem H.R., 1964, Plasma Spectroscopy, McGraw-Hill Book Company, New York

Griem H.R., 1974, Spectral Line Broadening by Plasmas, Academic Press, New York and London
Groth H.G., Kudritzki R.P., Butler K., et al., 1990, in: Garmany C.D. (ed.), Properties of hot luminous stars, San Francisco: ASP
Herrero A., Kudritzki R.P., Smartt S.J., et al., 2000, in: Bergeron J., Renzini A. (eds.), From Extrasolar Planets to Cosmology: The VLT Opening Symposium, Springer Verlag
Hoffleit D., 1982, The Bright Star Catalogue, New Haven: Yale Univ. Obs.
Hubeny I., Lanz T., 1993, in: Dworetsky M.M., Castelli F., Faraggiana R. (eds.), Peculiar Versus Normal Phenomena in A-Type and Related Stars, San Francisco: ASP
Husfeld D., Butler K., Heber U., Drilling J.S., 1989, A&A, 222, 150
Kaufer A., Stahl O., Wolf B., et al., 1996a, A&A, 305, 887
Kaufer A., Stahl O., Wolf B., et al., 1996b, A&A, 314, 599
Kaufer A., Stahl O., Tubbesing S., et al., 1999, The ESO Messenger 95, 8
Kaufman V., Martin W.C., 1991, J. Phys. Chem. Ref. Data, 20, 83
Kim D.-S., Tayal S.S., 2000, J. Phys. B, 33, 3235
Kondo Y., Talent D.L., Barker E.S., et al., 1978, ApJ, 220, L97
Kudritzki R.P., 1973, A&A, 28, 103
Kudritzki R.P., 1988, in: Chmielewski Y., Lanz T. (eds.), 18th Advanced Course of the Swiss Society of Astrophysics and Astronomy (Saas-Fee Courses): Radiation in Moving Gaseous Media, Geneva Observatory
Kurucz R.L., 1979, ApJS, 40, 1
Kurucz R.L., 1991, in: Crivellari L. et al. (eds.), Stellar Atmospheres: Beyond Classical Models, NATO ASI Ser. C-152, p. 441
Kurucz R.L., 1992, Rev. Mex. Astrofis., 23, 45
Kurucz R.L., Bell B., 1995, Kurucz CD-ROM No. 23, Smithsonian Astrophysical Observatory, Cambridge, Mass.
Kurucz R.L., Peytremann E., 1975, A Table of Semiempirical gf-values, Smithsonian Astrophys. Obs. Special Rept. No. 362
Lallement R., Ferlet R., Lagrange A.M., et al., 1995, A&A, 304, 461
Lambert D.L., Hinkle K.H., Luck R.E., 1988, ApJ, 333, 917
Lamers H.J.G.L.M., Snow T.P., Lindholm D.M., 1995, ApJ, 455, 269
Lemke M., Venn K.A., 1996, A&A, 309, 558
Lobel A., Achmad L., de Jager C., Nieuwenhuijzen H., 1992, A&A, 256, 159
Martin G.A., Fuhr J.R., Wiese W.L., 1988, J. Phys. & Chem. Ref. Data, Vol. 17, Suppl. 3
Martin W.C., Zalubas R., 1980, J. Phys. Chem. Ref. Data, 9, 1
McErlean N.D., Lennon D.J., Dufton P.L., 1998, A&A, 329, 613
McCarthy J.K., Kudritzki R.P., Lennon D.J., et al., 1997, ApJ, 482, 757
Mendoza C., Zeippen C.J., 1987, A&A, 179, 339
Mihalas D., 1972, ApJ, 177, 115
Mihalas D., 1978, Stellar Atmospheres (2nd ed.), W.H. Freeman and Company, San Francisco
Moccia R., Spizzo P., 1988, J. Phys. B., 21, 1133
Pfeiffer M.J., Frank C., Baumüller D., et al., 1998, A&AS, 130, 381
Przybilla N., 1997, Diplomarbeit, Ludwig Maximilians Universität, München
Przybilla N., Butler K., Becker S.R., et al., 2000, A&A, 359, 1085
Przybilla N., Butler K., Kudritzki R.P., 2001a, in preparation
Przybilla N., Butler K., Kudritzki R.P., 2001b, in preparation
Rogerson J.B., Jr., 1989, ApJS, 71, 1011
Rybicki G.B., Hummer D.G., 1991, A&A, 245, 171
Sadakane K., Nishimura M., 1979, PASJ, 31, 481
Sadakane K., Nishimura M., 1981, PASJ, 33, 189
Santolaya-Rey A.E., Puls J., Herrero A., 1997, A&A, 323, 488
Seaton M.J., 1962, in: Atomic and Molecular Processes, Academic Press, New York
Seaton M.J., Yu Y., Mihalas D., Pradhan A.K., 1994, MNRAS 266, 805
Sigut T.A.A., Lester J.B., 1996, ApJ, 461, 972
Sigut T.A.A., Pradhan A.K., 1995, J. Phys. B, 28, 4879
Simon T., Landsman W.B., 1997, ApJ, 483, 435
Snijders M.A.J., Lamers H.J.G.L.M., 1975, A&A, 41, 245
Talavera A., Gómez de Castro A.I., A&A, 181, 314
Van Regemorter H., 1962, ApJ, 136, 906
Venn K.A., 1995, ApJS, 99, 659
Venn K.A., 1999, ApJ, 518, 405
Venn K.A., Lambert D.L., 1990, ApJ, 363, 234
Venn K.A., McCarthy J.K., Lennon D.J., et al., 2000, ApJ, 541, 610
Venn K.A., Lennon D.J., Kaufer A., et al., 2001, ApJ, accepted
Verdugo E., Talavera A., Gómez de Castro A.I., A&AS, 137, 351
Vidal C.R., Cooper J., Smith E.W., 1973, ApJS, 25, 37
Wiese W.L., Smith W.M., Miles B.M., 1969, Atomic Transition Probabilities, Vol. II, NSRDS-NBS 22, Washington, D.C.
Wolf B., 1971, A&A, 10, 383
Zhao G., Butler K., Gehren T., 1998, A&A, 333, 219